Available online at www.sciencedirect.com
SCIENCE DIRECT
Thermochimica Acta 436 (2005) 15–25
thermochimica acta
www.elsevier.com/locate/tca

Full deconvolution of the instrumental coefficients in scanning calorimeter of heat flux type

Akihiko Toda*, Masamichi Hikosaka

Faculty of Integrated Arts and Sciences, Hiroshima University, 1-7-1 Kagamiyama, Higashi-Hiroshima 739-8521, Japan

Received 9 May 2005; received in revised form 27 June 2005; accepted 27 June 2005
Available online 8 August 2005

Abstract

A new method of full deconvolution of the instrumental coefficients in scanning calorimeter of heat flux type has been proposed, including reasonable determination method of the thermal contact resistance between the sample pan and its stage. The determination utilizes the response of dynamic heat capacity obtained by temperature-modulated (T-M) mode of a commercial differential scanning calorimeter used as a single calorimeter. By taking into account of the contribution of heat exchange with purge gas, an extension of standard modeling has been proposed for the evaluation of the instrumental coefficients. An alternative method bypassing the full deconvolution is also proposed.

Keywords: Modeling; Heat exchange with purge gas; Thermal contact resistance

1. Introduction

Reasonable determination method of instrumental coefficients is one of important issues in the quantitative thermal analysis with differential scanning calorimetry (DSC) of heat flux type. As a promising approach of the quantitative analysis, Danley [1] recently proposed a method (T4P method in Tzero^{TM} of TA Instruments) to construct the temperature of a sample pan and its heat flow from the raw data of temperatures at the sample stage and at the heat source without the information from a reference side. In his method aiming at the DSC of twin calorimeter, the same procedure is applied to the reference side, and then the heat flow from the sample is determined from the difference in heat flow between sample and reference sides.

For that purpose, the instrumental coefficients, such as the heat capacity of the sample stage, C_s, and the thermal contact resistance between the sample stage and the heat source, R_s, and between the sample stage and the sample pan, R_p, (and the corresponding coefficients for the reference side) have to be pre-determined. It has been demonstrated that C_s and R_s (and the corresponding coefficients for the reference side) can be reasonably determined from linear heating data with standard samples [1].

On the other hand, for the determination of the thermal contact resistance between the sample pan and its stage, R_p, he has assumed that there are two parallel heat conduction paths between the pan and the sensor through the solid surfaces in contact and through the gas in the interstices, and then formulated a model equation to calculate the contact resistance. For the thermal conductivities of each component employed in the modeling, empirical values are evaluated from literature data, and the geometric factors for the pan, sensor or purge gas have been determined from a multivariate curve fit of experimental data. By this procedure, we need to assume the same value of the contact resistance for each type of pan (both on sample and reference side) though there may be a scatter for individual pans.

In order to determine R_p directly, an attempt [2] has been undertaken by modeling the melting transition of pure metal [3], such as indium, and examining the response of the instrument. However, the obtained contact resistance is for the sample pan with the examined metal in it. Therefore, we had to assume that the resistance would be similar for all sample pans.

Basically, Danley's method indicated the possibility of quantitative analysis by a single calorimeter without utilizing

* Corresponding author. Tel.: +81 82 424 6558; fax: +81 82 424 0757.
E-mail address: atoda@hiroshima-u.ac.jp (A. Toda).

0040-6031/$ – see front matter © 2005 Elsevier B.V. All rights reserved.
doi:10.1016/j.tca.2005.06.037

the information from the reference. However, as will be discussed below, we have noticed that the modeling proposed by Danley does not account for the experimental results of the dynamic heat capacity obtained by temperature-modulated (T-M) mode even with standard samples, when a commercial DSC is used as a single calorimeter. Therefore, an extension of the modeling is proposed in the present paper in order to resolve the discrepancy. Analyzing the response of the dynamic heat capacity in terms of the new modeling, reasonable determination method of R_p can be provided. The method is applicable to all sample pans with target materials in them.

In the following, the method proposed by Danley is briefly reviewed, and then an extension of the modeling is proposed for the DSC used as a single calorimeter. The applicability of the new method is examined with the melting kinetics of polyethylene crystals by T-M mode and with the melting transitions of indium and polyethylene by conventional mode with linear heating.

2. Modeling

2.1. Mraw's model

The method proposed by Danley [1] is based on the Mraw's model of DSC of heat flux type [4]. In a DSC of heat flux type, the temperature at a heat source is controlled, and the sample temperature is detected at the stage which has a close contact with the sample pan. Following the Mraw's model [4], DSC of heat flux type is modeled as a lumped parameter circuit by the thermal resistances and the heat capacities of those parts shown in Fig. 1a. Then, the equations describing the heat flow at the sample side are expressed as follows:

$$C_s \frac{dT_s}{dt} + \frac{1}{R_p}(T_s - T_p) + \frac{1}{R_s}(T_s - T_0) = 0 \quad (1)$$

$$C_p \frac{dT_p}{dt} - F + \frac{1}{R_p}(T_p - T_s) = 0 \quad (2)$$

where T_s, T_0 and T_p represent the temperatures of sample stage, heat source (furnace) and sample pan, respectively, and C_s and C_p are the heat capacities of sample stage and that of sample + sample pan, respectively. The resistances of heat transfer between the heat source and the sample stage and between the sample stage and the sample pan are represented as R_s and R_p, respectively. Absorbed or released heat flow of kinetics is represented by F with negative sign for endothermic process.

Among them, available data are the temperatures of sample stage, T_s, and of heat source, T_0. Our objective is to see the relationship between the temperature of sample pan, T_p, and the heat flow from sample pan, $\dot{q}_p$, defined as:

$$\dot{q}_p \equiv -C_p \frac{dT_p}{dt} + F \quad (3)$$

From the available data of T_s and $\Delta T_0 \equiv T_0 - T_s$ with the predetermined coefficients of C_s and R_s, we are able to obtain a heat flow, $\dot{q}_s$ defined as follows:

$$\dot{q}_s \equiv C_s \frac{dT_s}{dt} - \frac{1}{R_s}\Delta T_0 \quad (4)$$

which corresponds to $\dot{q}_p$ within the framework of the model described by Eqs. (1) and (2).

For the determination of C_s and R_s, we can utilize the relationship of $\dot{q}_s = \beta C_s - \Delta T_0/R_s = -\beta C_p$, which is derived from Eqs. (1), (2) and (4) for linear heating at the rate, β, with a standard sample of known heat capacity, C_p, and without kinetics, $F = 0$. The relation is rearranged as:

$$\frac{\Delta T_0}{\beta} = R_s(C_p + C_s) \quad (5)$$

With Eq. (5), the coefficients, C_s and R_s, can be determined from the slope and the intercept of the linear plot of $\Delta T_0/\beta$ against C_p; typical example is shown in Fig. 2.

If the value of R_p is available, sample temperature, T_p, is obtained from T_s and $\dot{q}_s$ by Eqs. (1) and (4) as:

$$T_p = T_s + R_p \dot{q}_s \quad (6)$$

For the evaluation of R_p, Danley assumed two parallel heat conduction paths between the pan and the sensor through the solid surfaces in contact and through the gas in the interstices and suggested to utilize the literature values for the thermal conductivities of each component [1]. However, since R_p represents the thermal contact resistance between sample pan and its stage, the value will be dependent on the condition of the contact and will have to be determined

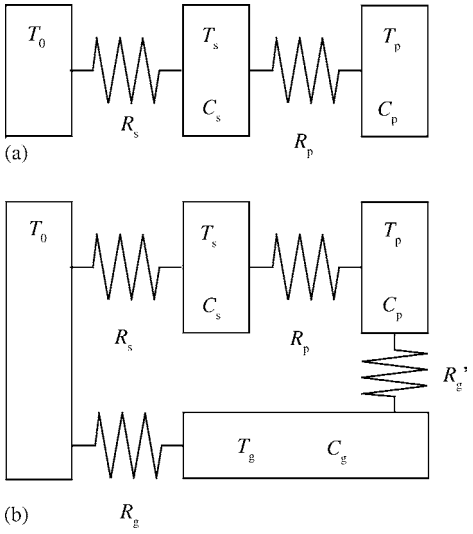

Fig. 1. (a) Schematic representation of the Mraw's model describing a DSC of heat flux type for the sample side: temperatures of the heat source T_0, the sample stage T_s and the sample pan T_p. R_s and R_p represents the thermal resistance. The heat capacities of the sample stage and sample + sample pan are represented as C_s and C_p, respectively. (b) The extension of the Mraw's model with the contribution of heat exchange with purge gas.

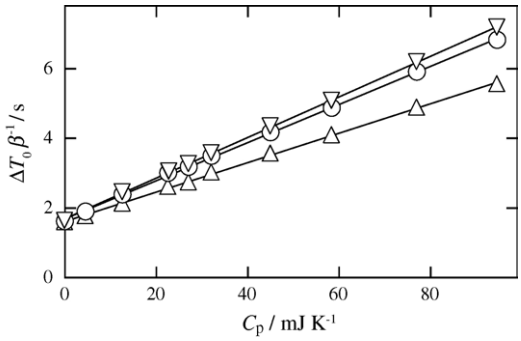

Fig. 2. Plots of $\Delta T_0\beta^{-1}$ against sample heat capacity, C_p, with the purge gases of: nitrogen (○); helium (△) and krypton (▽), following Eq. (5). The examined heating rate was 10 K min^{-1}.

for each sample pan. We propose the following method utilizing the response of dynamic heat capacity obtained by temperature-modulated mode for the DSC used as a single calorimeter.

Temperature-modulated mode of DSC (T-M DSC) applies a periodic modulation in sample temperature and examines the response in heat flow [5–10]. The response is represented by a dynamic heat capacity of complex quantity, and the raw data of the dynamic heat capacity, $\tilde{C}_{\mathrm{raw}}\mathrm{e}^{-\mathrm{i}\varphi}$, is given by the ratio of the modulation components, as follows:

$$\tilde{C}_{\mathrm{raw}}\mathrm{e}^{-\mathrm{i}\varphi} = \frac{i}{\omega}\frac{\tilde{\dot{q}}_{\mathrm{s}}}{\tilde{T}_{\mathrm{s}}}\mathrm{e}^{-i(\epsilon_{\mathrm{s}}-\delta_{\mathrm{s}})} \tag{7}$$

where $Re[\tilde{\dot{q}}_{\mathrm{s}}\mathrm{e}^{i(\omega t+\delta_{\mathrm{s}})}]$ and $Re[\tilde{T}_{\mathrm{s}}\mathrm{e}^{i(\omega t+\epsilon_{\mathrm{s}})}]$ represent the modulation components of $\dot{q}_{\mathrm{s}}$ and T_{s}, respectively, with the angular frequency, $\omega = 2\pi/(\mathrm{Period})$. From Eqs. (1), (2), (4) and (7), $\tilde{C}_{\mathrm{raw}}\mathrm{e}^{-\mathrm{i}\varphi}$ is given as:

$$\tilde{C}_{\mathrm{raw}}\mathrm{e}^{-\mathrm{i}\varphi} = (C_{\mathrm{p}}^{-1} + i\omega R_{\mathrm{p}})^{-1} \tag{8}$$

and hence, the real and imaginary parts of the following expressions will give C_{p}^{-1} and R_{p}, respectively;

$$\tilde{C}_{\mathrm{raw}}^{-1}\mathrm{e}^{\mathrm{i}\varphi} = C_{\mathrm{p}}^{-1} + i\omega R_{\mathrm{p}} \tag{9}$$

$$(\omega\tilde{C}_{\mathrm{raw}})^{-1}\mathrm{e}^{\mathrm{i}\varphi} = (\omega C_{\mathrm{p}})^{-1} + iR_{\mathrm{p}} \tag{10}$$

Fig. 3 shows an example of the attempt by the plots against angular frequency of modulation, ω, of the dynamic heat capacity obtained by temperature-modulated mode with the DSC used as a single calorimeter. The data points in each plot should be on a horizontal line determined by the values of C_{p}^{-1} (the real part of Eq. (9) corresponding to Fig. 3a) and R_{p} (the imaginary part of Eq. (10) corresponding to Fig. 3b), respectively, and hence the coeffcient, R_{p}, may be determined by this plot. However, neither of the plots in Fig. 3 follows this expectation from Eqs. (9) and (10). This result clearly indicates that the Mraw's model misses an important factor to describe real single calorimeter and we will not be able to rely on this model to evaluate R_{p}.

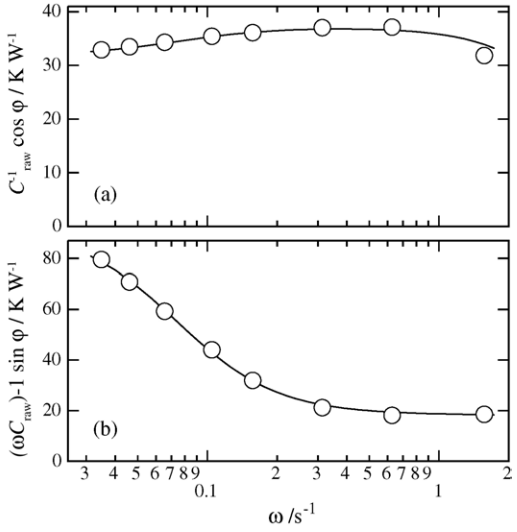

Fig. 3. Plots of: (a) C_{raw}^{-1} cos φ and (b) $(\omega C_{\mathrm{raw}})^{-1}$ sin φ against log ω, which correspond to the real part of Eq. (9) and the imaginary part of Eq. (10), respectively: quasi-isothermal at 142 °C with the amplitude of ±0.2 °C. Sample was aluminum of 31.5 mJ K^{-1}. Purge gas was nitrogen. The curved lines represent the result of the fitting with Eq. (22).

2.2. Heat exchange with purge gas

The subject of the Mraw's model has been a twin calorimeter utilizing both of the sample and reference sides. For a single calorimeter, in order to explain the discrepancy of the plots in Fig. 3 from the behaviors expected with Eqs. (9) and (10) and to propose reasonable method of R_{p} determination, we make an attempt to extend the Mraw's model to incorporate the heat exchange with purge gas, which has been neglected in the original Mraw's model. Concerned with the purge gas, in addition to Eq. (1) for the sample stage, we must consider the following Eq. (11) instead of Eq. (2) for the sample pan and Eq. (12) for the purge gas, respectively,

$$C_{\mathrm{s}}\frac{\mathrm{d}T_{\mathrm{s}}}{\mathrm{d}t} + \frac{1}{R_{\mathrm{p}}}(T_{\mathrm{s}} - T_{\mathrm{p}}) + \frac{1}{R_{\mathrm{s}}}(T_{\mathrm{s}} - T_0) = 0 \tag{1}$$

$$C_{\mathrm{p}}\frac{\mathrm{d}T_{\mathrm{p}}}{\mathrm{d}t} - F + \frac{1}{R_{\mathrm{p}}}(T_{\mathrm{p}} - T_{\mathrm{s}}) + \frac{1}{R'_{\mathrm{g}}}(T_{\mathrm{p}} - T_{\mathrm{g}}) = 0 \tag{11}$$

$$C_{\mathrm{g}}\frac{\mathrm{d}T_{\mathrm{g}}}{\mathrm{d}t} + \frac{1}{R'_{\mathrm{g}}}(T_{\mathrm{g}} - T_{\mathrm{p}}) + \frac{1}{R_{\mathrm{g}}}(T_{\mathrm{g}} - T_0) = 0 \tag{12}$$

where T_{g} represents the average temperature of purge gas, C_{g} the effective heat capacity of purge gas which contributes to the heat exchange, and R_{g} and R'_{g} the effective thermal resistances of heat transfer between the purge gas and the heat source and between the purge gas and the sample pan, respectively (Fig. 1b). The resistances, R_{g} and R'_{g}, will represent the coefficients in any type of heat transfer, such as conduction, radiation and convection, if the temperature difference is small enough. For the resistances, the relationship of $R'_{\mathrm{g}} \gg R_{\mathrm{g}}$ will be satisfied under general conditions be-

cause the inner area of furnace is much larger than the surface area of sample pan and hence the heat exchange with heat source (furnace) will dominate the exchange with sample pan. It is also expected that $R'_g \gg R_s, R_p$ due to closer contact between heat source and sample stage and between sample stage and sample pan than the contact through the purge gas for R'_g.

For linear heating under steady state without kinetics, namely for $F = 0$ and $\dot{T}_0 = \dot{T}_s = \dot{T}_p = \dot{T}_g = \beta$, from Eqs. (1), (11) and (12), the relationship between $\Delta T_0/\beta$ and C_p is represented as follows for $R'_g \gg R_g, R_s, R_p$,

$$\frac{\Delta T_0}{\beta} \cong R_s[C_p + C_s + C_g^0] \tag{13}$$

$$C_g^0 \equiv \frac{R_g C_g - R_s C_s}{R'_g} \tag{14}$$

Therefore, the coefficients, R_s and $C_s + C_g^0$, are determined from the linear plot of $\Delta T_0/\beta$ against C_p. Then, instead of $\dot{q}_s$ in Eq. (4), we obtain the following $\dot{q}'_s$ from the available data:

$$\dot{q}'_s \equiv (C_s + C_g^0)\frac{dT_s}{dt} - \frac{\Delta T_0}{R_s} = \dot{q}_s + C_g^0\frac{dT_s}{dt} \tag{15}$$

under the condition of $F = 0$ and $\dot{T}_0 = \dot{T}_s = \dot{T}_p = \dot{T}_g = \beta$, $\dot{q}'_s$ gives the correct value for the contribution of sample heat capacity to the heat flow; namely, $\dot{q}'_s \cong -\beta C_p$ from Eqs. (13)–(15).

Under general conditions without the restrictions, the temperature of purge gas, T_g, is obtained from Eq. (12) as:

$$T_g = \frac{1}{\tau'}\int_{-\infty}^{t} e^{-(t-t')/\tau'}\frac{R'_g T_0 + R_g T_p}{R_g + R'_g}dt' \tag{16}$$

$$\tau' = \frac{R_g R'_g}{R_g + R'_g}C_g \tag{17}$$

In terms of periodic temperature modulation, Eq. (16) gives the following expression of the modulation component of the temperature of purge gas:

$$\tilde{T}_g e^{i(\omega t+\epsilon_g)} = \frac{1}{1+i\omega\tau'}\frac{R'_g\tilde{T}_0 e^{i(\omega t+\epsilon_0)} + R_g\tilde{T}_p e^{i(\omega t+\epsilon_p)}}{R_g + R'_g} \tag{18}$$

and hence the relationship between the raw data of the dynamic heat capacity, $\tilde{C}_{raw}e^{-i\varphi}$, and the true heat capacity of sample, C_p, is given as follows:

$$\tilde{C}_{raw}e^{-i\varphi} = \frac{i}{\omega}\frac{\tilde{q}'_s}{\tilde{T}_s}e^{-i(\epsilon_s-\delta'_s)} = \left[\left(C_p + \frac{C''_g}{1+i\omega\tau''}\right)^{-1} + i\omega R_p\right]^{-1} - C_g^0 \tag{19}$$

$$\tau'' = \frac{R_g R'_g C_g + R_p R_s C_s}{R_g + R'_g + R_p + R_s} \tag{20}$$

$$C''_g = \frac{R_g C_g - R_s C_s - (R_p + R_s)C_p - i\omega R_p C_p R_s C_s}{R_g + R'_g + R_p + R_s} \cong C_g^0 - (m_1 + i\omega m_2)C_p \quad \text{for} \quad R'_g \gg R_g, R_p, R_s \tag{21}$$

where $\tau'' \cong \tau' \cong R_g C_g \cong R'_g C_g^0$, $m_1 \equiv (R_p + R_s)/R'_g \ll 1$ and $m_2 \equiv R_p R_s C_s/R'_g \ll 1$ for $R'_g \gg R_g, R_p, R_s$ because $R_s C_s \sim 1$ s with DSC Q1000, as shown below. Therefore, if we assume that the term, $(m_1 + i\omega m_2)C_p$, is negligible under the conditions of $R'_g \gg R_g, R_p, R_s$ and $m_1, \omega m_2 \ll 1$, the relationship is further approximated as:

$$\tilde{C}_{raw}e^{-i\varphi} \cong \left[\left(C_p + \frac{C_g^0}{1+i\omega\tau'}\right)^{-1} + i\omega R_p\right]^{-1} - C_g^0 \tag{22}$$

The fitting with this expression to the experimental data shown in Fig. 3 is satisfactory, and the coefficients, R_p, τ' and C_g^0, can be reasonably determined by the fitting.

Figs. 4 and 5 show the temperature dependence of those coefficients determined by this procedure. Firstly, Fig. 4 shows the decrease in the thermal resistance, R_s, and the increase in the heat capacity, $C_s + C_g^0$, with increasing temperature. Small dependence on purge gas of those coefficients will be due to heat transfer between purge gas and the path connecting the heat source and the sample stage.

On the other hand, it is clearly seen in Fig. 5a that the thermal contact resistance between sample pan and its stage, R_p, is strongly dependent on the choice of purge gas due to the large contribution of the heat transfer via the purge gas between the surfaces; the thermal conductivity of krypton, nitrogen and helium gases at room temperature are 9.4×10^{-3}, 2.6×10^{-2} and 1.5×10^{-1} $Wm^{-1}K^{-1}$, respectively. The temperature dependence of R_p with krypton purge gas shows a decrease following the temperature dependence of the thermal conductivity of the gas. However, the dependence with nitrogen is almost negligible and that of helium shows a posi-

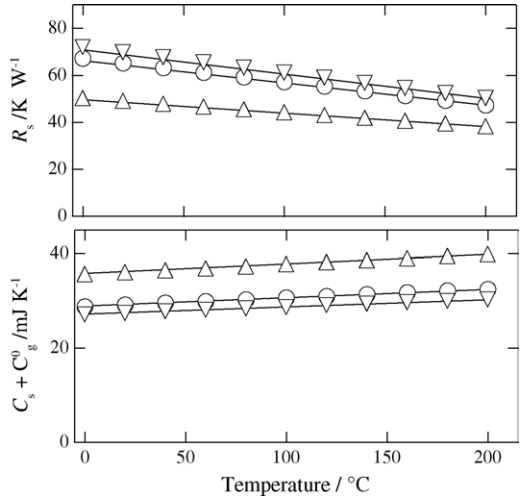

Fig. 4. Plots of the coefficients, R_s, and $C_s + C_g^0$, against temperature with the purge gases of: nitrogen (○); helium (△) and krypton (▽).

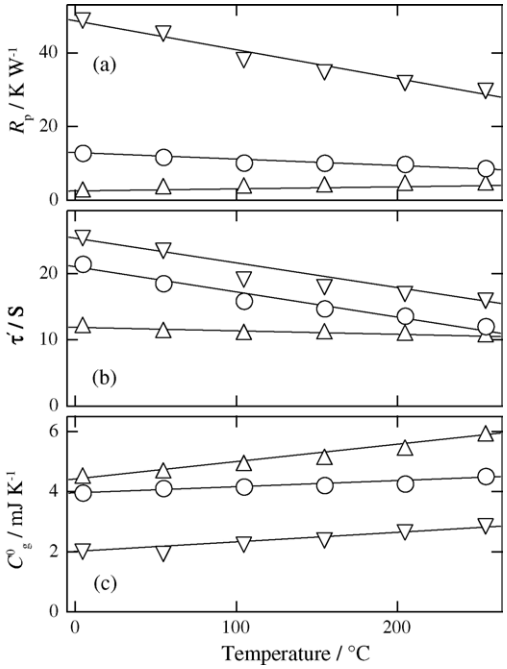

Fig. 5. Plots of the coefficients, R_p, τ' and C_g^0, against temperature with the purge gases of: nitrogen (○); helium (△) and krypton (▽). Sample was aluminum of 28.41 mg.

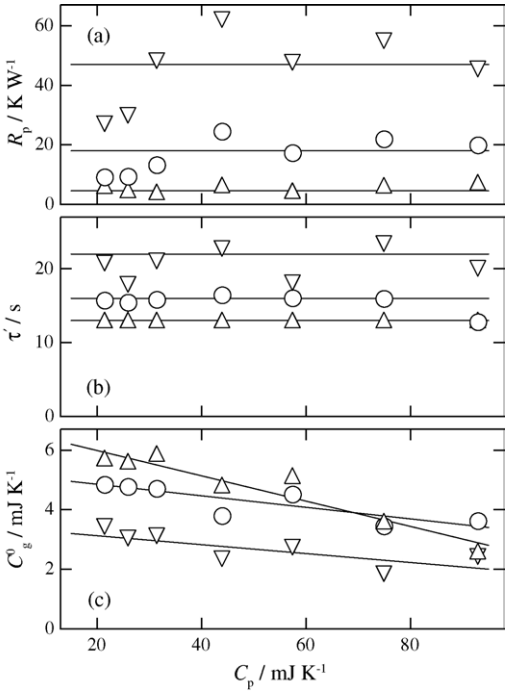

Fig. 6. Plots of the coefficients, R_p, τ' and C_g^0, against sample heat capacity with the purge gases of: nitrogen (○); helium (△) and krypton (▽). Sample was aluminum of 23.90–99.00 mg. The examined temperature was 142 °C.

tive dependence, though the absolute values are much smaller than that with krypton. Those behaviors with purge gases having smaller thermal conductivity indicate the contributions of not only the thermal conductivity of those gases but also the direct thermal contact between the pan and its stage, which can be variable with each sample pan and even with each stage because of the contamination of the stage. In this sense, the determination of R_p for each instrument with each sample pan is strongly appreciated. In terms of the characteristic time, τ', shown in Fig. 5b, τ' becomes shorter with increasing temperature for all purge gases. Finally, the basic trend of the heat capacity, C_g^0, in Fig. 5c is an increasing function of temperature.

Based on the results shown in Figs. 4 and 5, we can confirm the relationship assumed in the above. Firstly, it is indicated that $R_sC_s \sim 1$ s for all purge gases in the examined temperature range because $R_s \sim 50\,\mathrm{KW}^{-1}$, $C_s + C_g^0 \sim 30\,\mathrm{mJ\,K}^{-1}$, and $C_s \gg C_g^0$. Secondly, R_g' is given as $R_g' = \tau'/C_g^0$, and the value was about 3000–6000 KW^{-1} which is actually much larger than $R_s \sim 50\,\mathrm{KW}^{-1}$ and $R_p \leq 50\,\mathrm{KW}^{-1}$ in the examined temperature range shown in Figs. 4 and 5.

Concerned with the assumption of $m_1, m_2 \ll 1$ in Eq. (21), Fig. 6 shows the coefficients, R_p, τ' and C_g^0, obtained by the fitting for aluminum samples with different mass in a wide range. In Fig. 6c, we see the systematic decrease in C_g^0 with increasing sample heat capacity, C_p, as expected for C_g'' in Eq. (21). The dependence is determined by the magnitude of the coefficient, $m_1 + i\omega m_2$, which was estimated as −0.043, −0.019 and −0.016 for helium, nitrogen and krypton gases, respectively, from the slopes of the plots in Fig. 6c. Therefore, the condition of $m_1 \ll 1$ and $m_2 \lesssim m_1 \ll 1$ will be satisfied. Strictly speaking, the assumption of $(m_1 + i\omega m_2)C_p \ll C_g^0$ for Eq. (22) is not satisfied specifically for He purge gas, as seen in Fig. 6c. Because of the term, $(m_1 + i\omega m_2)C_p$, in Eq. (21), the C_p determination by use of the relationship of Eq. (22) will have an error of at most 4, 2 and 2% for helium, nitrogen and krypton gases, respectively. In terms of the behaviors of R_p and τ' in Fig. 6a and b, basically, they depend not on the sample heat capacity but on the choice of the purge gas, as expected; the scattering of R_p in Fig. 6a will be due to the change in the condition of thermal contact between the surfaces of sample pan and its stage for different sample pans.

In summary, under the condition of $R_g' \gg R_g$, R_p, R_s, the procedure of the deconvolution by use of the DSC as a single calorimeter is summarized as follows:

1. For linear heating without kinetics: $F = 0$ and $\dot{T}_0 = \dot{T}_s = \dot{T}_p = \dot{T}_g = \beta$, the relationship of Eq. (13) holds.

$$\frac{\Delta T_0}{\beta} \cong R_s[C_p + C_s + C_g^0] \tag{13}$$

   The linear plot of $\Delta T_0/\beta$ against C_p of standard samples is utilized for the determination of R_s and $C_s + C_g^0$.
2. From the raw data of T_s and ΔT_0 with predetermined coefficients, R_s and $C_s + C_g^0$, the obtainable heat flow of the

single calorimeter is $\dot{q}'_s$ represented as Eq. (15).

$$\dot{q}'_s \equiv (C_s + C_g^0)\frac{dT_s}{dt} - \frac{\Delta T_0}{R_s} \tag{15}$$

3. By the temperature-modulated mode of the single calorimeter, the raw data of the dynamic heat capacity, $\tilde{C}_{raw}e^{-i\varphi}$, is given as Eq. (22).

$$\tilde{C}_{raw}e^{-i\varphi} \cong \left[\left(C_p + \frac{C_g^0}{1+i\omega\tau'}\right)^{-1} + i\omega R_p\right]^{-1} - C_g^0 \tag{22}$$

Examining the frequency dependence, the coefficients, R_p, τ' and C_g^0, of each sample pan can be determined from the fitting such as shown in Fig. 3

When using the DSC as a single calorimeter, the true heat flow from the sample pan, $\dot{q}_p$, and the temperature of the sample pan, T_p, can be determined from the experimentally obtainable heat flow, $\dot{q}'_s$, and temperatures, T_s and T_0, with those coefficients predetermined by this procedure. If the same procedure is done for the reference side as a twin calorimeter, the difference in heat flow gives the heat flow from the sample itself.

Concerned with the importance of the heat exchange with purge gas, it needs to be mentioned that the heat exchange will be the same at both of the sample and reference sides for a twin calorimeter, when the sample and reference sides are exactly symmetric, including the heat capacities of both sides. For the symmetric case, the heat exchange with gas will therefore be canceled out when taking the difference, and hence the above procedure may not be necessary. However, on the occasion of a phase transition or a chemical reaction, the effective heat capacity of the sample can undergo significant change due to the heat of transition or chemical reaction, and hence the symmetric heat exchange with gas cannot be guaranteed. This will be the reason why it is recommended to apply different cell constants for the measurement of heat capacity (symmetric case) and for that of heat of transition or chemical reaction (asymmetric case). Therefore, in general, the full deconvolution including the heat exchange with gas will be required even for the conventional DSC with the symmetric twin arrangement of the sample and reference sides, when a phase transition or a chemical reaction is examined. For this reason, we prefer simpler method using the DSC as a single calorimeter in the following discussion.

For the DSC used as a single calorimeter to examine kinetics by linear heating ($F \neq 0$ and $\dot{T}_0 = \beta$), the true heat flow from sample pan, $\dot{q}_p$, and the temperature of the sample pan, T_p, are given by the experimentally obtainable heat flow, $\dot{q}'_s$, and temperatures, T_s and T_0, from Eqs. (1), (3), (4), (11) and (16), as follows:

$$T_p = T_s + R_p\left(\dot{q}'_s - C_g^0\frac{dT_s}{dt}\right) \tag{23}$$

$$\begin{aligned}\dot{q}_p &= \dot{q}'_s - C_g^0\frac{dT_s}{dt} + \frac{1}{R_g + R'_g} \\ &\quad\times\left(T_p - T_0 + \beta\tau' + \frac{R_g}{R'_g}\int_{-\infty}^{t} e^{-(t-t')/\tau'}\dot{T}_p dt'\right) \\ &\cong \dot{q}'_s - C_g^0\frac{dT_s}{dt} + \frac{1}{R'_g}(T_p - T_0 + \beta\tau') \quad \text{for} \quad R'_g \gg R_g\end{aligned} \tag{24}$$

where the coefficients, R_p, τ', C_g^0 and $R'_g(\cong \tau'/C_g^0)$, are predetermined outside the transition region.

On the other hand, with temperature-modulated mode, the true effective heat capacity, $\widetilde{\Delta C}\,e^{-i\alpha}$, in a transition region with the contribution of kinetics is deconvoluted from the raw data, $\tilde{C}_{raw}e^{-i\varphi}$, obtained by temperature-modulated mode as:

$$\widetilde{\Delta C}\,e^{-i\alpha} = [(\tilde{C}_{raw}e^{-i\varphi} + C_g^0)^{-1} - i\omega R_p]^{-1} - \frac{C_g^0}{1+i\omega\tau'} \tag{25}$$

with the coefficients, R_p, τ' and C_g^0, predetermined outside the transition region by Eq. (22); those coefficients are basically determined by the outer surface of sample pan, and hence we assume that the values will not be strongly modified by the kinetics in the sample pan.

3. Experimental

A Q1000^{TM} DSC (TA Instruments) with a refrigerated cooling system installed was used for all measurements. Helium, nitrogen and krypton gases with a flow rate of 10 mL min^{-1} were purged through the cell; the small flow rate is to reduce temperature perturbation by the purge gas in the furnace. Reference pan was removed in all experiments because we use the DSC as a single calorimeter without the temperature data from the reference side. The sampling interval was limited at 0.2 s.

In the determination of the coefficients, R_s and $C_s + C_g$, with Eq. (13), we need standard sample with known heat capacity. In the experiments shown above, we utilized a disk-shaped thin sheet of aluminum (4.70 mg in weight, 95 μm thick) and the sample heat capacity was varied by changing the number of the sheets in the sample pan, which is also made of aluminum.

For the determination of R_p, τ' and C_g^0 of each sample pan, the fitting with the expression of Eq. (22) to the experimental data such as shown in Fig. 3 was performed by the Levenberg–Marquardt algorithm [11] of non-linear and least-squares fitting provided with Igor Pro 4 program (Wave Metrics, Inc.).

The applicability of the present method to the complex heat capacity obtained with T-M mode was examined with the melting kinetics of polyethylene, which was NIST SRM1475 of $M_w = 5.2 \times 10^4$ and $M_w/M_n = 2.9$. On the other hand, the applicability to the linear heating in conventional mode

was examined with the melting of indium and polyethylene. Samples were cut into the shape of a disk to fit the interior of sample pan in order to avoid the deformation of the aluminum pan on crimping. The thickness of polyethylene sample was around 100 μm.

For the periodic modulation in temperature, a saw-tooth pattern of temperature modulation was applied with the period in the range of 4–180 s. On heating, the amplitude was set to satisfy "heating only" condition, $\dot{T}_s > 0$.

4. Application to the melting kinetics of polymers by temperature-modulated mode

We are able to see the response of melting kinetics appearing in the effective heat capacity obtained by a periodic modulation in sample temperature with underlying linear heating controlled as $T = T_0 + \beta t + Re[\tilde{T}\, e^{i(\omega t+\epsilon)}]$, where β represents the rate of underlying linear heating. For the melting kinetics of polymer crystals, we have experimentally confirmed that the response is roughly approximated as a frequency response function of Debye's type [12,13],

$$\widetilde{\Delta C}\, e^{-i\alpha} \equiv \widetilde{\Delta C}' - i\widetilde{\Delta C}'' \cong C_p + \frac{-\bar{F}/\beta}{1 + i\omega\tau_m(\beta)} \qquad (26)$$

where $\bar{F}$ represents the mean endothermic heat flow on melting, which is included in "total" heat flow determined by averaging modulated heat flow over one period. The characteristic time, τ_m, represents the quickness of the melting kinetics and corresponds to the mean time required from the onset of melting until its completion. Due to faster increase in ΔT with faster underlying heating rate, β, the characteristic time, τ_m, becomes shorter with faster β.

In order to obtain the true effective heat capacity on melting, the instrumental time constants need to be deconvoluted. Eq. (25) provides the automatic deconvolution for the complex heat capacity. Fig. 7 shows the typical raw data in the melting region of polyethylene crystals with the modulation periods of 10–120 s. It is clearly seen that the deconvolution is really necessary especially for the phase angle of the complex heat capacity, which must be zero outside the melting region. Fig. 8 shows the real and imaginary parts of the effective heat capacity after the full deconvolution by Eq. (25) with the coefficients, R_p, τ' and C_g^0, predetermined by quasi-isothermal T-M mode at both sides of the melting region. The successful deconvolution is indicated basically by the behaviors outside the melting region: no frequency dependence and negligibly small values of the imaginary parts.

Fig. 9 shows the comparison of the frequency dependence of the real and imaginary parts of the effective heat capacity, such as shown in Fig. 8, at the peak temperature obtained with different purge gases. The agreement among the results was within 5% except for the imaginary part with the shortest modulation period of 10 s. Therefore, the agreement is satisfactory in terms of the determination of the characteristic

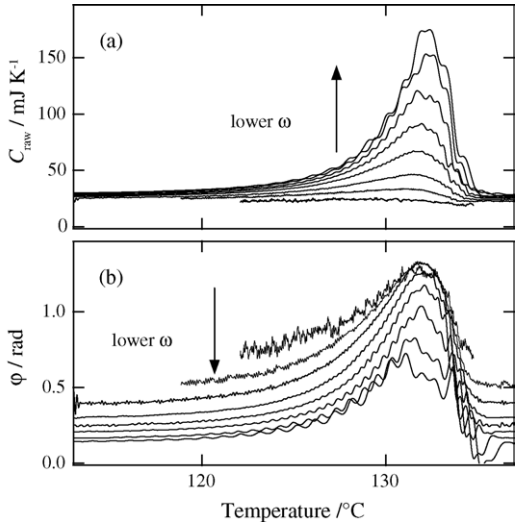

Fig. 7. Plots of the raw data of the: (a) magnitude and (b) phase angle of the effective heat capacity in the melting region of polyethylene. Modulation periods were 9.6, 14.4, 20.4, 30, 42, 60, 90 and 120 s. Underlying heating rate was 1.0 K min^{-1} and a heating-only condition was applied. Sample mass was 3.31 mg. Purge gas was nitrogen.

time of melting kinetics, τ_m, which is obtained from the peak frequency of the imaginary part, ω^{peak}, by the expression of $\omega^{peak}\tau_m = 1$. The agreement confirms the successful deconvolution of the instrumental time constants, which should be strongly affected by the thermal conductivity of the purge gas. On the other hand, Fig. 10 shows the results of a trial of alternative deconvolution of the raw data, $\tilde{C}_{raw}e^{-i\varphi}$, shown in Fig. 7 by the following expression for the magnitude of

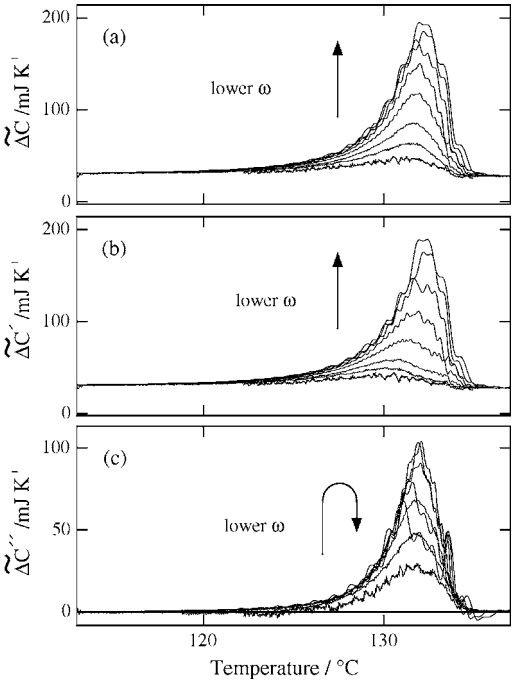

Fig. 8. Plots of the: (a) magnitude; (b) real and (c) imaginary parts of the effective heat capacity deconvoluted from the raw data in Fig. 7.

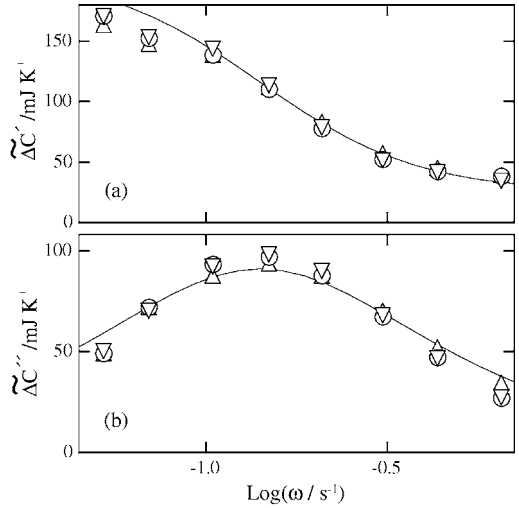

Fig. 9. Frequency dependence of the: (a) real and (b) imaginary parts of the effective heat capacity taken at the peak temperature in the plots such as shown in Fig. 8 with purge gases of: nitrogen (○); helium (△) and krypton (▽).

the heat capacity, $\widetilde{\Delta C}$, and by the baseline subtraction for the phase angle;

$$\frac{1}{\tilde{C}_{\mathrm{raw}}} = \frac{1}{\widetilde{\Delta C}}[1 + A\omega^2]^{1/2} \tag{27}$$

where A is a constant. As shown in Fig. 10, though the simpler method has been utilized in previous works, the method works only with helium purge gas, with which the thermal contact resistance, R_p, is the lowest among the purge gases examined.

In the present deconvolution method, we have assumed that the coefficients utilized for the deconvolution is not affected by the change inside the sample pan because those coefficients are concerned with the outer surface of the sample pan. However, it is expected that the thermal contact between polymers and aluminum sample pan undergoes a large change on melting, and the change may have small influence on the determination of those coefficients. In order to examine the effect on the coefficients, we examined the coefficients in the melting region at several temperatures by quasi-isothermal T-M mode. In the melting region, the sample was annealed for 20 min before the measurements at the respective temperatures. Fig. 11 shows the results of C_p, R_p, τ' and C_g^0 determined by the fitting to Eq. (22). In the melting region shown in Fig. 11a, we can recognize the peak in C_p, which is assigned to the response of a reversible process. The reversible process can be comprised of complex processes, and the basic research has been done by Wunderlich's group [14,15]. In terms of those coefficients, R_p, τ' and C_g^0, determined by the present method, there is a small stepwise change in C_g and R_p by about 5–10%, as shown in Fig. 11b. Since they are stepwise changes, we can interpolate the coefficients determined at both sides of the melting region with the change in crystallinity in the melting region. Even though the small change in the coefficients does not cause significant error in the obtained results, it is therefore recommended to determine those coefficients at both sides and to use the interpolated values in the melting region.

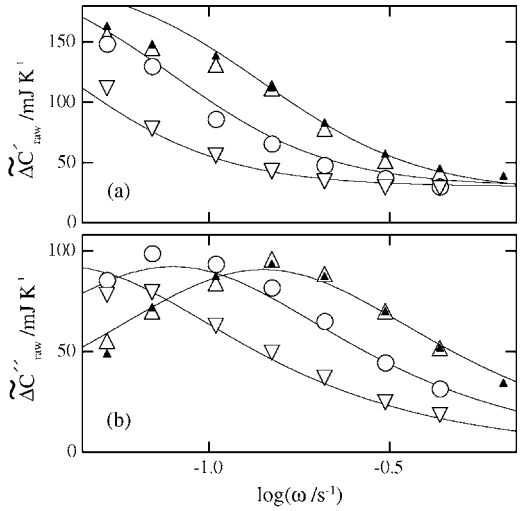

Fig. 10. Frequency dependence of the: (a) real and (b) imaginary parts of the effective heat capacity calculated from the raw data such as shown in Fig. 7 by Eq. (27) for the magnitude and by the baseline subtraction for the phase angle. Purge gases were: nitrogen (○); helium (△) and krypton (▽). The symbol (▲) represents the properly deconvoluted ones with helium purge gas shown in Fig. 9.

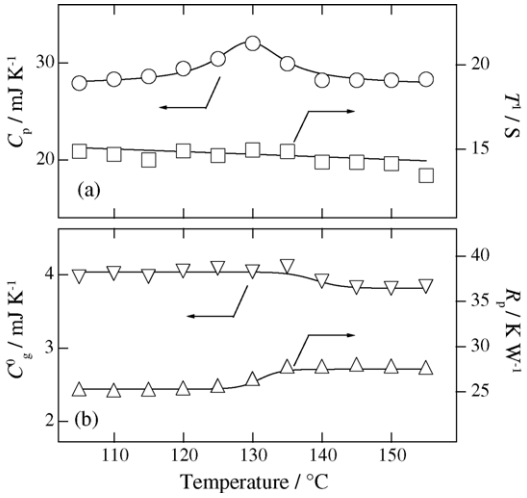

Fig. 11. Plots of the sample heat capacity, C_p, and the coefficients, τ', C_g^0 and R_p, against temperature. The values were determined with polyethylene sample (2.47 mg) in the temperatures covering the melting region. Purge gas was nitrogen.

5. Application to the melting by linear heating mode

In order to further confirm the validity and the applicability of the deconvolution, we examine the melting with conventional mode of linear heating. A pure metal standard such as indium is supposed to melt at a single transition point with negligibly small superheating. Then, the deconvoluted tem-

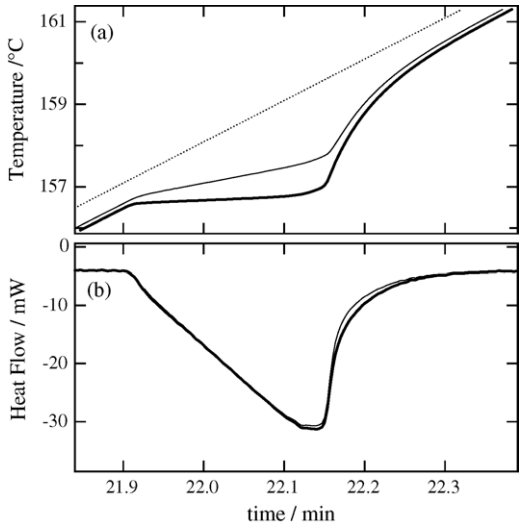

Fig. 12. Plots of: (a) temperature and (b) heat flow against time in the melting of indium (9.98 mg). In (a), thick line represents T_p, thin line T_s and dotted line T_0. In (b), thick line represents $\dot{q}_p$ and thin line $\dot{q}_s$. Heating rate was 10 K min^{-1}. Purge gas was nitrogen.

perature of sample pan, T_p, will stay at the melting temperature; even in a case with small temperature gradient in the sample pan, the temperature rise will be quite small. Then, we firstly examine the melting transition of indium.

The full deconvolution of T_p and $\dot{q}_p$ from T_s and q'_s was made by Eqs. (23) and (24) with the coefficients, R_p, τ' and C_g^0, predetermined by quasi-isothermal T-M mode at both sides of the melting transition of indium. The obtained results are shown in Fig. 12a, in which the temperature rise of the deconvoluted T_p during the melting is actually quite small in comparison with the measured temperature at the sample stage, T_s. On the other hand, Fig. 12b shows the measured heat flow $\dot{q}'_s$ and the deconvoluted one, $\dot{q}_p$; the difference between them is quite small.

With the sample temperature, T_p, the instrumental time constants is automatically deconvoluted. This feature is quite useful in examining the melting temperature and the kinetics of the system having broad melting region; the typical example is the melting of polymer crystals. Fig. 13 shows the example of the melting region of polyethylene crystals. In the plots, we remove the contribution of $-C_p\dot{T}_p$, which is estimated from the heat flow outside the melting region (baseline), from $\dot{q}_p$ in Eq. (3). Pure contribution of heat flow on melting, F, is plotted against T_p. As a trial, similar heat flow F' is calculated from $\dot{q}'_s$ by removing the baseline of the outside, $-C_p\dot{T}_s$, and is plotted against T_s in Fig. 13; F' and T_s are available from the measured data without the deconvolution procedure. The shift in the melting peak temperature due to the difference between T_p and T_s is clearly seen, while the difference in heat flows is quite small.

In order to evaluate the true melting temperature and the melting kinetics, it is required to examine the heating rate dependence of the peak temperature, $T_p^{peak}(\beta)$, which shows

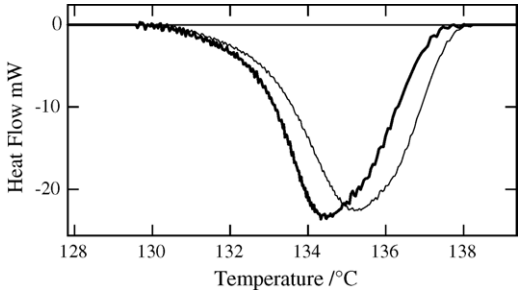

Fig. 13. Plots of heat flow on melting of polyethylene crystals against temperature; thick line represents the plots of F vs. T_p and thin line F' vs. T_s. Heating rate was 10 K min^{-1}. Sample mass was 2.47 mg. Purge gas was nitrogen.

the following dependence [2]:

$$T_p^{peak}(\beta) - T_p^{peak}(0) \propto \beta^{-x} \tag{28}$$

where $T_p^{peak}(0)$ corresponds to the true melting peak temperature of the sample without superheating, and the power x is determined by the superheating dependence of the melting rate. This kind of data is only available after the deconvolution of the instrumental time constants.

6. An alternative method bypassing the full deconvolution

We have seen that, in the T-M mode, the evaluation of the magnitude of the heat capacity by Eq. (27) and the baseline subtraction of phase angle worked satisfactory only with helium purge gas. With other gases of nitrogen and krypton, the results gave wrong characteristic time of melting kinetics, τ_m, in Eq. (26), which is determined from the peak frequency of the imaginary part as shown in Figs. 9 and 10. On the other hand, in terms of the deconvolution of sample temperature T_p from T_s, there is no such alternative method.

Among the instrumental coefficients, R_p, τ' and C_g^0, the most influential coefficient is R_p. Therefore, if we can significantly reduce the thermal contact resistance between the bottom of sample pan and its stage, we will be able to bypass the deconvolution procedure. For this purpose, we applied silicone grease (Archer, 276–1372) between the surfaces. Then, we evaluated the value of R_p with the present method and examined the melting of polymer crystals with T-M mode and the melting of indium with conventional mode by linear heating.

Firstly, Fig. 14 shows the evaluated coefficients, τ' and C_g^0, with the standard sample of aluminum. In terms of R_p, the value became less than 10^{-3} KW^{-1} for all purge gases and was practically assumed to be zero. The results indicate significant effect of the application of silicone grease to the thermal contact resistance, while the values of τ' and C_g^0, which are related with the heat exchange of sample pan with purge gas, remain to be similar to those shown in Fig. 5.

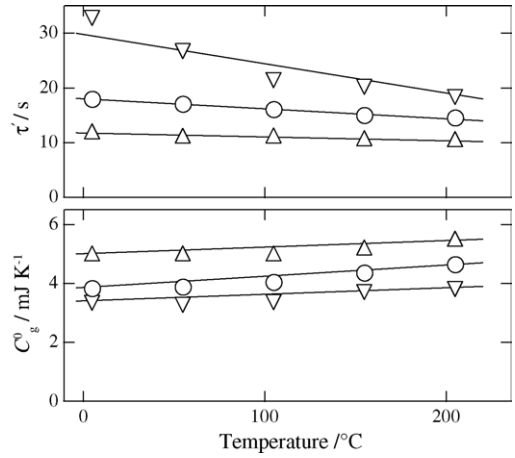

Fig. 14. Plots of the coefficients, τ' and C_g^0 against temperature. The coefficients were determined with the application of silicone grease at the contact surface of sample pan and its stage. The symbols and other conditions are the same as in Fig. 5.

Secondly, the raw data of T-M mode in the melting region of polyethylene is shown in Fig. 15. With the silicone grease, it is seen that, outside the melting region, the phase angle becomes much closer to zero compared with the case shown in Fig. 7; the remaining deviation from zero is due to the heat exchange with the purge gas. Fig. 16 shows the comparison of the results of the correct deconvolution method with helium purge gas and the alternative method utilizing Eq. (27) and the baseline subtraction of the phase angle with three purge gases. In this case, the simpler method with Eq. (27) and baseline subtraction works well for all purge gases with the application of silicone grease.

Finally, in terms of T_p and T_s in the course of the melting of indium with linear heating, the difference becomes negligible

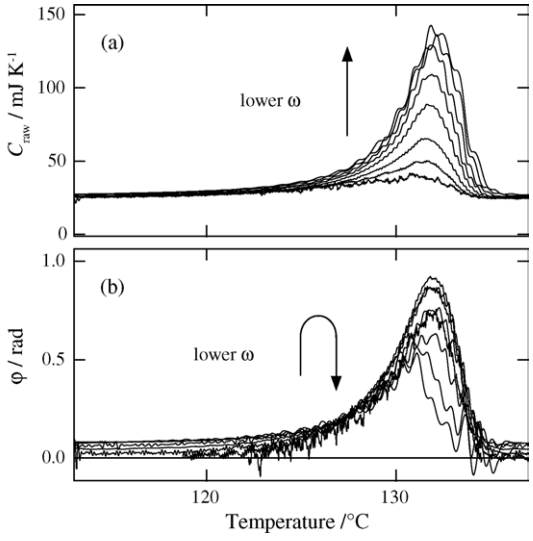

Fig. 15. Plots of the raw data of the: (a) magnitude and (b) phase angle of the effective heat capacity in the melting region of polyethylene with the silicone grease at the contact surface of sample pan and its stage. Conditions are the same as in Fig. 7.

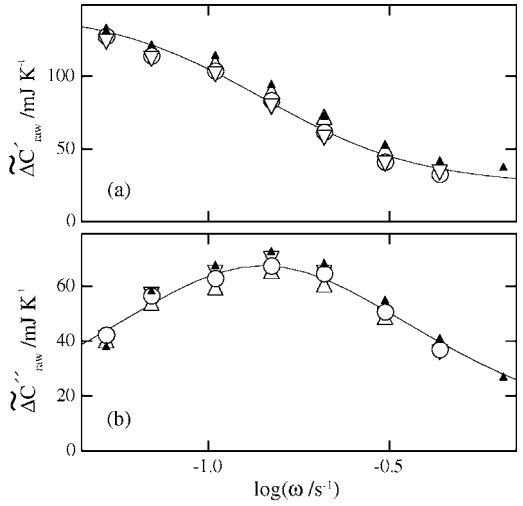

Fig. 16. Frequency dependence of the: (a) real and (b) imaginary parts of the effective heat capacity calculated from the raw data shown in Fig. 15 The symbols and other conditions are the same as in Fig. 10.

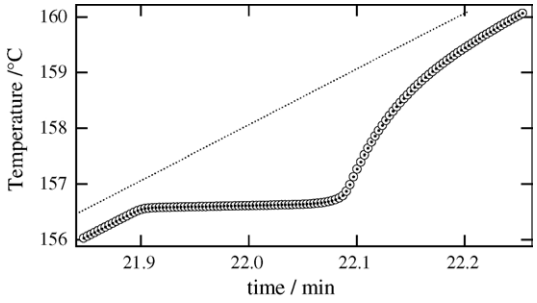

Fig. 17. Plots of temperature against time in the melting of indium with silicone grease at the contact surface of sample pan and its stage; T_p (○) and T_s (●) and dotted line T_0. Conditions are the same as in Fig. 12.

with the application of silicone grease, as shown in Fig. 17, because of the negligibly small value of the thermal contact resistance between the bottom of sample pan and its stage.

All those results show that the application of silicone grease can actually bypass the correct deconvolution method for both of T-M mode and conventional mode.

7. Discussion and conclusion

In the present paper, a new method of full deconvolution of instrumental coefficients has been proposed, utilizing the response of the dynamic heat capacity obtained by temperature-modulated mode with the DSC used as a single calorimeter, which does not utilize the temperature data at the reference side. Since the original Mraw's model aimed at a twin calorimeter and did not explain the behaviors of the raw data of the dynamic heat capacity obtained by the single calorimeter, we extended the model to incorporate the heat exchange with surrounding purge gas. The fitting to the

expression of the heat capacity was satisfactory, and the instrumental coefficients were reasonably determined by the fitting.

With the predetermined coefficients, the dynamic heat capacity determined by temperature-modulated mode with the single calorimeter can be automatically deconvoluted as the true effective heat capacity even in the course of transformation kinetics. The method was applied to the melting kinetics of polyethylene, and we confirmed the successful agreement of the results with different purge gases having different values of the coefficients. A simpler method of deconvolution utilizing the calibration of the magnitude by Eq. (27) and baseline subtraction for phase angle works satisfactory only with helium purge gas, which has the highest thermal conductivity.

The method is then applied to the melting kinetics by linear heating of conventional mode with the single calorimeter. For the case of the melting of indium which is a typical standard material, the deconvoluted temperature of sample pan, T_p, kept nearly constant value during the melting transition in comparison with the steady increase in the temperature of the sample stage, T_s. In terms of the melting region of polyethylene, the deconvolution procedure automatically subtracts the shift in peak temperature due to the instrumental thermal lag, and hence we can analyze the melting kinetics quantitatively by use of the deconvolution procedure.

An alternative method has also been proposed, which bypasses the full deconvolution by applying silicone grease to the contact surface of sample pan and its stage. With better thermal conductivity of silicone grease in comparison with purge gas between the surfaces, the thermal contact resistance between the surfaces became negligibly small. Then, the simpler method with Eq. (27) and with the baseline subtraction of phase angle worked satisfactory for all purge gases examined by T-M mode in the melting region of polyethylene crystals. For conventional mode by linear heating, the difference between the deconvoluted sample temperature, T_p, and the measured temperature at the stage, T_s, becomes negligible with the application of silicone grease. Therefore, the full deconvolution of the instrumental coefficients will be reasonably bypassed by this method. The trial of the application of silicone grease has been proposed before, but the quantitative analysis with the evaluation of the thermal contact resistance between the surfaces has been realized by the present method of full deconvolution for the first time.

Finally, it is noted that the influence of the heat exchange with purge gas may be neglected for a conventional DSC used as a twin calorimeter because the heat exchange occurs both at the sample and at the reference sides and is cancelled out when taking the difference between the temperature data at the sample and reference sides for the case of exactly symmetric heat flow, i.e. for the baseline of heat flow. However, on the occasion of phase transitions and chemical reactions, the heat flow exchanging with gas will be out of balance due to the temperature difference caused by the heat of transitions and chemical reactions (asymmetric case). For this reason, the present method considering the heat exchange with purge gas will be more preferable for the examination of transition kinetics and chemical reactions, in general. The influence will be significant for the dynamic heat capacity determined by temperature-modulated mode as seen in the above. For the conventional mode by linear heating, the difference in heat flow between $\dot{q}'_s$ and $\dot{q}_p$ on transition was quite small, and hence the benefit of the deconvolution mainly lies in the determination of true sample temperature, T_p. Finally, the alternative method of the application of silicone grease to the contact surface can bypass the full deconvolution and has the outcome practically equivalent to the full deconvolution.

Acknowledgement

The author thanks Mr. N. Urayama (TA Instruments Japan Inc.) for providing the access to DSC Q1000.

References

[1] R.L. Danley, Thermochim. Acta 395 (2003) 201–208.
[2] A. Toda, K. Yamada, M. Hikosaka, Polymer 43 (2002) 1667–1679.
[3] Y. Saito, K. Saito, T. Atake, Thermochim. Acta 99 (1986) 299–307.
[4] S.C. Mraw, Rev. Sci. Instrum. 53 (1982) 228–231.
[5] P.S. Gill, S.R. Sauerbrunn, M. Reading, J. Therm. Anal. 40 (1993) 931–939.
[6] M. Reading, D. Elliott, V.L. Hill, J. Therm. Anal. 40 (1993) 949–955.
[7] M. Reading, A. Luget, R. Wilson, Thermochim. Acta 238 (1994) 295–307.
[8] B. Wunderlich, Y. Jin, A. Boller, Thermochim. Acta 238 (1994) 277–293.
[9] A. Boller, Y. Jin, B. Wunderlich, J. Therm. Anal. 42 (1994) 307–330.
[10] I. Hatta, Jpn. J. Appl. Phys. 33 (1994) 686–688.
[11] W.H. Press, B.P. Flannery, S.A. Teukolsky, W.T. Vetterling, Numerical Recipes in C, Cambridge University Press, Cambridge, 1988 (Chapter 14).
[12] A. Toda, C. Tomita, M. Hikosaka, Y. Saruyama, Polymer 39 (1998) 5093–5104.
[13] A. Toda, T. Arita, C. Tomita, M. Hikosaka, Thermochim. Acta 330 (1999) 75–83.
[14] I. Okazaki, B. Wunderlich, Macromolecules 30 (1997) 1758–1764.
[15] K. Ishikiriyama, B. Wunderlich, Macromolecules 30 (1997) 4126–4131.